Beyond the Universal Volume Scaling: Tailoring Two-Photon Absorption in Nanomaterials by Heterostructure Design

Arthur Alo,[1] *Leonardo W.T. Barros,*[1] *Gabriel Nagamine,*[1] *Jonathan C. Lemus,*[1] *Josep Planelles,*[2] *José L. Movilla,*[3] *Juan I. Climente,*[2] *Hak June Lee,*[4,5] *Wan Ki Bae,*[5] *and Lazaro A. Padilha* [1*]

[1]*Instituto de Fisica "Gleb Wataghin", Universidade Estadual de Campinas, UNICAMP, P.O. Box 6165, 13083-859 Campinas, Sao Paulo, Brazil*

[2]*Dept. de Química Física i Analítica, Universitat Jaume I, 12080, Castelló, Spain;*

[3]*Dept. d'Educació i Didàctiques Específiques, Universitat Jaume I, 12080, Castelló, Spain;*

[4]*School of Chemical and Biological Engineering, Seoul National University, Seoul 08826, Republic of Korea;*

[5]*SKKU Advanced Institute of Nanotechnology (SAINT), Sungkyunkwan University (SKKU), Suwon 16419, Republic of Korea*

e-mail: padilha@ifi.unicamp.br

Abstract

Colloidal semiconductor nanomaterials present broadband, large cross-section, and two-photon absorption (2PA) spectra, which turns them into an important platform for applications that benefit from high nonlinear optical response. Despite that, to date, the only means to control the magnitude of the 2PA cross-section is by changing the nanoparticle volume, as it follows a universal volume scale, independently of the material composition. As the emission spectrum is connected utterly to the nanomaterial dimensions, for a given material, the magnitude of the nonlinear optical response is also coupled to the emission spectral. Here, we demonstrate means to decouple both effects by exploring the 2PA response of different types of heterostructures, tailoring the volume dependence of the 2PA cross-section due to different dependence of the density of final states on the nanoparticle volume. By heterostructure engineering, one can obtain one order of magnitude enhancement of the 2PA cross-section with minimum emission spectra shift.

Keywords:

Nonlinear optics; quantum dots; nanocrystals; CdSe; up-conversion; ultrafast spectroscopy

On the crusade to find materials with high nonlinear optical (NLO) responses, semiconductor nanomaterials emerged as promising candidates. Theoretical models for two-photon absorption, 2PA, suggested that the oscillator strength for a single 2PA transition increases with quantum confinement.[1-3] However, it has been shown that the measured value for 2PA cross-section, σ_{2PA}, at the quasi-continuum spectral range in semiconductor quantum dots, QDs, depends linearly on the nanomaterial volume. The decrease in the overall σ_{2PA} for smaller QDs results from the drastic reduction in the density of states caused by quantum confinement.[4-6] PbS QDs, which combines narrow bulk band gap with small and symmetric electron and hole effective masses, are the first demonstration of quantum confinement-induced enhancement of σ_{2PA}.[7] However, the properties that allow for the enhancement of the NLO response in PbS QDs also change their bandgap as a function of the nanomaterial size. Consequently, changes in NLO response are connected to changes in the absorption and emission spectra, as they are dependent on the nanomaterial volume.

Several studies has been dedicated to decoupling the size dependence of the absorption and emission spectra in nanostructures. Among the strategies used, doping the nanomaterial to create a long-lived, red-shifted trap-mediated emission,[8,9] and nanomaterial heterostructuring by growing thick-shell of different materials[10,11] have proven to be successful in this task. Methods for nanomaterials heterostructuring have been developed over the last decade to reduce excitons non-radiative decay channels, by passivating trap sites, and by reducing Auger recombination rate via electron delocalization.[12-15] Nevertheless little is known about the NLO response of these heterostructured nanocrystals (NCs). Naturally, the questions that emerge are how different types of band alignment affect their NLO response, and if it is possible to manipulate the nanomaterial NLO response without drastically changing their emission

spectra. If so, what would be the best strategy to have the maximum 2PA enhancement for a given emission spectral range?

To address those questions, here, we have investigated the size dependence of σ_{2PA} for different types of CdSe-based heterostructures, which include bare core CdSe QDs, type-I CdSe/CdZnS core/shell, and quasi-type-II CdSe/CdS core/shell NCs. In a previous work, we have shown that for type-I band alignment, the volume scaling for σ_{2PA} is broken and a sub-linear volume dependence is observed.[16] Here, we show that for quasi-type-II heterostructures, the volume dependence of σ_{2PA} changes with the ratio between the core and shell dimensions in a way that it can be optimized to obtain about one order of magnitude enhancement on σ_{2PA} for samples emitting at similar wavelengths.

The samples studied are: CdSe core-only QDs with radii varying between 1.5 and 3.0 nm, synthesized following the route described in Ref. [17]; CdSe/CdZnS type-I core/shell with fixed core radius (r) of 2.0 nm and shell thicknesses (H) varying from 1.2 to 4.2 nm, synthesized according to the method of Ref. [18]; and two series of quasi-type-II CdSe/CdS core/shell (r = 2.0 nm, 1.5 nm ≤ H ≤ 5.5 nm and r = 1.5 nm, 2.0 nm ≤ H ≤ 5.0 nm), synthesized following the procedure described in Ref. [14]. **Figure 1a** compares literature values for σ_{2PA} for different visible-emitting QDs, including core-only CdSe QDs, evidencing the linear correspondence between σ_{2PA} and volume. Absorption and photoluminescence (PL) spectra for the core-only and core/shell samples with core radius of 2.0 nm are shown in **Figure 1 (b-d)**. As seen in **Figure 1 (c, d)**, increasing the shell thickness barely changes the PL spectra for both type-I and quasi-type-II structures.

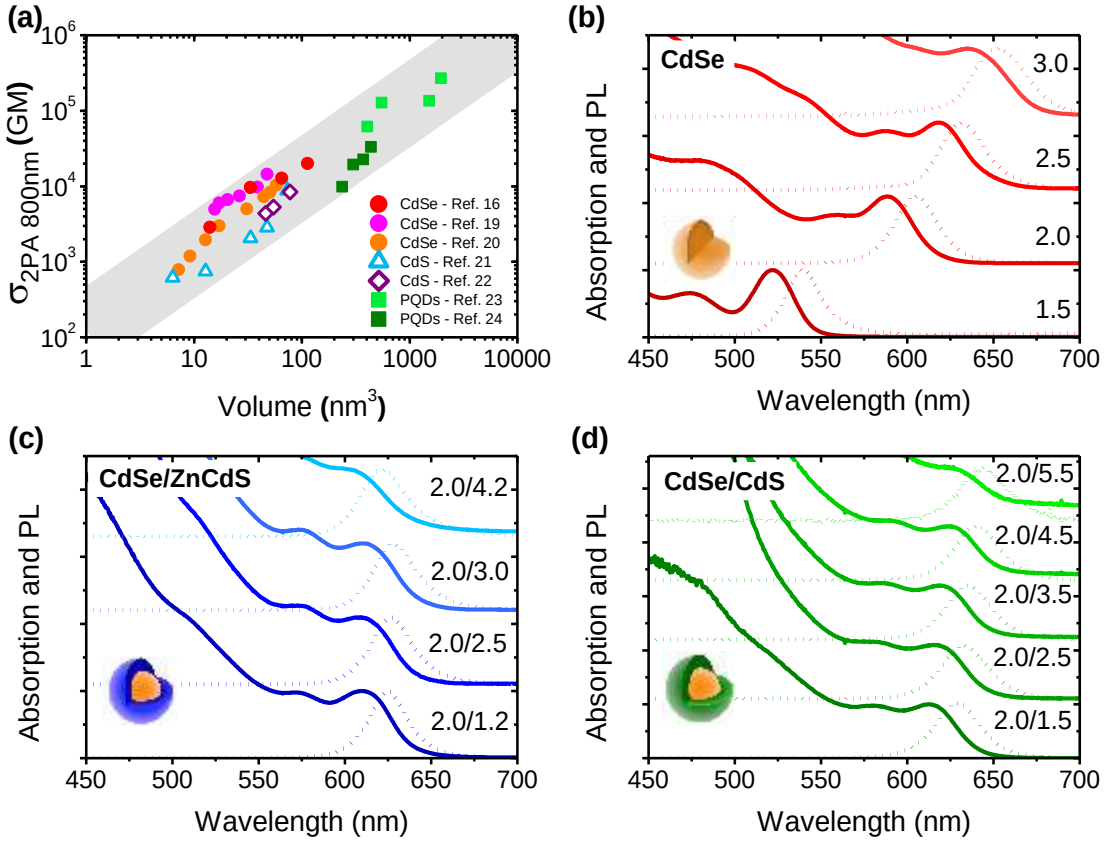

Figure 1. (a) Two-photon absorption cross section measured with excitation at 800 nm for core-only quantum dots as a function of the volume, with data from Refs. [16, 19-24] (values shown for σ_{2PA} are not corrected by the local field penetration). At the quasi-continuum spectral range, σ_{2PA} grows linearly with the nanoparticle volume, as shown by the shaded area (linear curve with $\sigma_{2PA} \propto V^{1.0}$). Absorption and emission spectra for (b) CdSe, (c) CdSe/ZnCdS, and (d) CdSe/CdS nanocrystals with their core/shell radius/thickness indicated in nanometers.

All values for σ_{2PA} were measured using the multi-photon absorption by photoluminescence saturation technique (MPAPS),[16] as it allows for accurate determination of the volume dependence for nonlinear absorption in nanomaterials. 2PA spectra were obtained by two-photon excited photoluminescence (2PEP),[25] and the magnitude was obtained by considering the absolute values of σ_{2PA} measured with

MPAPS.[16] Details on the experimental methods, including the experimental data and fittings are in the SI.

Figures 2 (a, b) shows the 2PA spectra for a series of type-I (a) and quasi-type-II (b) CdSe-based heterostructures, all with a core radius of 2.0 nm and varying shell thicknesses. Changing the shell thickness influences σ_{2PA} magnitude mostly for high-energy transitions, independently of the type of band alignment. Near the band edge, due to the scarce density of transitions, the magnitude of the 2PA at each excitation wavelength is influenced by the shell thickness (due to small shifts on the band edge energy) and size distribution. Consequently, to eliminate the influences from size distribution and spectral shift, for fair comparison of the 2PA magnitude among different samples, in this case, it is appropriate to compare the spectrally integrated σ_{2PA}. Note that, the spectral integration in **Figure 2** is intended only to avoid misleading interpretation of the volume scaling due to spectral dependence of the 2PA near the core band edge. By spectrally integrating the 2PA spectra from **Figure 2 (a, b)** for energies above and below the shell band gap, we see that, for transition energies below the shell bandgap, the integrated σ_{2PA} is nearly volume independent for both types of band alignment, as shown in **Figures 2 (c, d)**. This is expected for type-I structures as, in this situation, the initial, final, and all most probable intermediate states are confined to the core (**Figure 2e**). For the quasi-type-II, the conduction band edge, i.e., the final state, expands to the core and shell (**Figure 2f**), and we would expect changes in σ_{2PA} with the volume, which, within the experimental error, is not observed. The most interesting features are observed for transition energies above the shell bandgap, for which initial and final states expand to the shell (**Figure 2g**). For both types of shell, σ_{2PA} increases with the shell thickness, however, the volume dependence is weaker for type-I than for quasi-type-II structures.

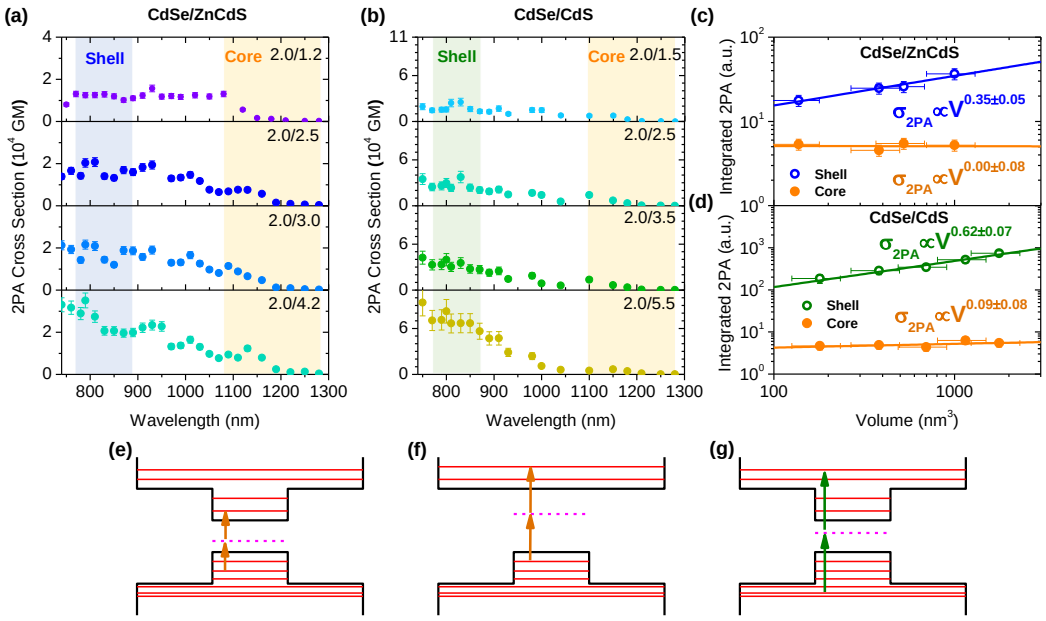

Figure 2. Two-photon absorption spectra for (a) type-I CdSe/ZnCdS (r = 2.0 nm, H = 1.2, 2.5, 3.0 and 4.2 nm)[16] and (b) quasi-type-II CdSe/CdS (r = 2.0 nm, H = 1.5, 2.5, 3.5 and 5.5 nm) core/shell samples. The dimensions of QDs (r/H) are noted in each panel of the figures. To verify how the 2PA magnitude changes with the nanomaterials volume, we integrate the two-photon absorption spectra for energies above the shell bandgap (shaded areas in blue of Figure 2a and green of Figure 2b) and near the core band edge, corresponding to the first 2PA transition peak (shaded areas in yellow) for (c) type-I and (d) quasi-type-II samples. (e) and (f) indicate the initial, intermediate, and final states for the first 2PA transition in type-I and quasi-type-II respectively. (g) For transitions above the shell bandgap, the initial and final states expand to the core and shell. The dashed lines in the bandgaps (in e,f,g) indicate the intermediate state, which are states in the valence or conduction bands, energy detuned, as shown in Eq. 1.

Figure 3 summarizes the volume dependence of σ_{2PA} measured at 800 nm (1.55 eV, i.e., above the shell bandgap, and within the spectral range in which the optical transitions form a quasi-continuum) for core-only, and core/shell type-I and quasi-type-

II nanostructures. While for core-only σ_{2PA} scales linearly with the volume, the dependence is $\sigma_{2PA} \propto V^{0.58}$ and $\sigma_{2PA} \propto V^{0.30}$ for quasi-type-II and type-I, respectively. All core/shell structures here have the same core radius, 2.0 nm. As expected, at the limit in which the shell thickness tends to zero, the values for σ_{2PA} for the core/shell samples tend to that of the core-only with 2.0 nm.

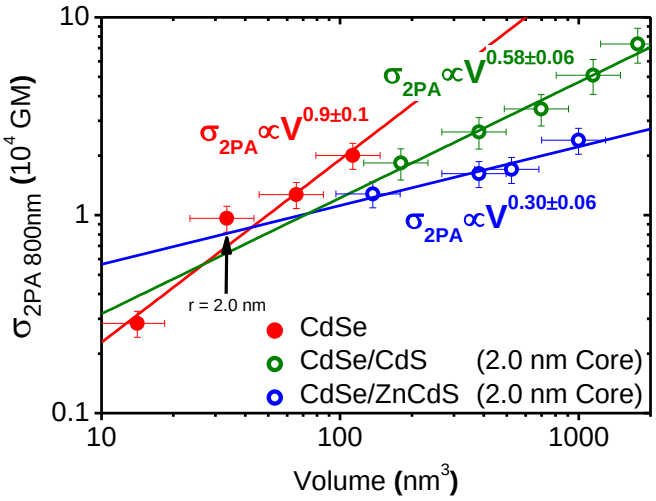

Figure 3. Measured σ_{2PA} at 800 nm as a function of the volume for the three sets of samples. For CdSe core only, σ_{2PA} scales linearly with the volume, as expected, while for the core/shell QDs, the dependence appears to be sublinear: $\sigma_{2PA} \propto V^{0.56}$ and $\sigma_{2PA} \propto V^{0.30}$ for quasi-type-II CdSe/CdS QDs and type-I CdSe/ZnCdS QDs, respectively.

To explain how different band alignments influence the σ_{2PA} volume dependence, we have performed calculations based on single-band $\vec{k} \cdot \vec{p}$ Hamiltonians for non-interacting electrons and holes. Similar models have successfully explained the main features of 2PA in core-only QDs and nanorods,[26,27] dot-in-rods,[28] and nanoplatelets.[29,30]

The 2PA cross section can be evaluated as $\sigma_{2PA} = W_{2PA}/I_{ph}^2$, in which I_{ph} is the photon flux density and W_{2PA} the two-photon transition rate. The latter is the key magnitude connecting the electronic structure with the observed 2PA spectrum. It can be estimated using second order Fermi golden rule:

$$W_{2PA}(h\nu) \propto \sum_{i,f} \left| \sum_m \frac{\langle f|\vec{e}\cdot\vec{p}|m\rangle\langle m|\vec{e}\cdot\vec{p}|i\rangle}{E_m - E_i - h\nu} \right|^2 \delta(E_f - E_i - 2h\nu), \quad (1)$$

where $|j\rangle$ stands for the wave function of the initial ($j=i$), intermediate ($j=m$), or final ($j=f$) state, with energy E_j. $\vec{e}$ is the light polarization vector and $\vec{p}$ is the momentum operator. For the excitations we observe, the matrix elements in Equation (1) involve one interband and one intraband transition. In our simulations, the delta function in Equation (1) is replaced by a Gaussian function of 40 meV width, which provides a simple description of the band broadening experienced by a single nanocrystal (arising e.g. from laser non-monochromaticity or dephasing, as well as thermal population distribution). Size dispersion, which is also present in the experiments and would deviate from the Gaussian profile, is neglected here because we aim at establishing a connection between well-defined NC size and composition and the resulting 2PA. In this regard, it is worth noting that the size dispersion in the core/shell experimental samples is typically on the order of 10%, while the range of diameter varies by more than a factor of 2. Then, no qualitative changes are expected in the connection between simulations and experiments if size dispersion was explicitly accounted for.

Because of the spherical symmetry of our NCs, electron and heavy hole states can be labeled as nL_q, where L denotes the envelope function angular momentum (*S, P, D*… for $L=0,1,2\ldots$), $q=e,h$ denotes the carrier (electron or hole) and n is the main quantum number. The selection rules impose that interband transitions take place between hole and

electron states with the same angular momentum L, while intraband ones do so between states with $\Delta L = (2k + 1)$,[28,31] with k an integer number. **Figure 4a** depicts schematically a couple of processes fulfilling such conditions (red and blue arrows).

The question we want to answer is what the effect of volume and band alignment is in determining σ_{2PA}. To this end, we need to identify the physical factors that influence W_{2PA} (and hence σ_{2PA}). This is most conveniently done by visualizing the low energy window of the spectrum, where the transitions are well resolved, rather than focusing on the quasi-continuum at 3.1 eV only. **Figure 4b** shows the calculated W_{2PA} for core-only CdSe QDs with increasing radius. Narrow peaks represent discrete transitions between hole and electron levels (delta function in Eq.(1)), while the enveloping bands simulate a broadened spectrum (Gaussian function), for qualitative comparison with the experiments. Several observations can be inferred from the figure. First, even though the angular momentum selection rule is $\Delta L = (2k + 1)$, in practice the peaks with large oscillator strength correspond to $\Delta L = \pm 1$ only (examples are given in the spectral assignment at low energies). Second, the oscillator strength of individual transitions decreases with increasing QD radius, cf. height of peaks in **Figure 4b** for increasing radius (**Figure 4d**). This is because the intraband momentum matrix elements in Equation (1) are of the form $\langle f|\vec{e}\cdot\vec{p}|m\rangle = \vec{e}\cdot\langle\chi_f|\vec{p}|\chi_f\rangle\langle u_f|u_f\rangle$, where χ_j and u_j stand for the envelope and cell-periodic (Bloch) function of the state *j,* and the envelope functions matrix element $\langle\chi_f|\vec{p}|\chi_f\rangle$ scales proportionally to *1/r.* Third, and most important, the enveloping W_{2PA} function for a given transition energy increases despite the smaller oscillator strength (**Figure 4d**). This is because of the higher density of states (DOS), which for a 3D box scales linearly with the volume,[30] with this effect prevailing over the reduced oscillator strength. In other words, it is the DOS of the final state (contained in the resonance condition of Eq.(1)), rather than the overlap between initial and final state

wave functions in the optical transition (matrix elements of Eq.(1)) that determines the trends of σ_{2PA}.

In **Figure 4c**, we compare the calculated W_{2PA} of a CdSe QD with a radius of 4 nm (bottom panel) and that of core/shell NCs with the same total dimension (r = 2.0/H = 2.0 nm), be it either CdSe/CdS (middle panel) or CdSe/ZnCdS (top panel). The DOS of the CdSe QD is higher than that of the CdSe/ZnCdS NC, which results in greater envelope W_{2PA}. The CdSe/CdS NC, in turn, has an intermediate DOS (notice the transitions are more closely-spaced than in CdSe/ZnCdS) and envelope W_{2PA}. The trend in **Figure 4c** is thus qualitatively consistent with the experimental observation that, for the same volume, σ_{2PA} in a CdSe QD is greater than that of CdSe/CdS NC, and this, in turn, is greater than that of CdSe/ZnCdS NCs.

The interpretation in terms of the electronic structure goes as follows. In CdSe QDs, the DOS of both electrons and holes increases with the total volume of the particle. In CdSe/ZnCdS NCs, however, the shell acts as a type-I potential barrier which allows for moderate tunneling of electrons and holes only. Thus, increasing the shell thickness provides only a small additional *effective* volume. CdSe/CdS NCs are an intermediate case because the quasi-type-II band alignment (with a shallow conduction band offset) enables significant electron (but not hole) delocalization with increasing shell thickness.

The above reasoning relies on the premise that the effect of the band alignment on W_{2PA} is mainly set by the DOS behavior. Evidence that the influence of the wave functions overlap (matrix elements in Eq.(1)) is a secondary effect is also found in **Figure 4c**. When comparing the oscillator strength of the discrete transitions in type-I (CdSe/ZnCdS) and quasi-type-II (CdSe/CdS) NCs, one can only see a moderate decrease (**Figure 4e**), which is compensated by the higher DOS to yield comparable or greater

envelope W_{2PA} (**Figure 4f**). Further insight into the secondary role of wave function overlaps is provided in the SI. To avoid the influence of the simulated size distribution on the magnitude of W_{2PA}, in **Figure 4f** we plot the integrated intensity of W_{2PA}, within the quasi-continuum spectral range, similarly to what is done in **Figure 2**. The integration is carried out in a region of 0.2 eV (2.9-3.1 eV), which is comparable to or greater than the inhomogeneous bandwidth in the experiments. The trend predicted for the integrated W_{2PA} is experimentally verified if we extrapolate from the fittings in **Figure 3** the values for σ_{2PA} for type-I (CdSe/ZnCdS), quasi-type-II (CdSe/CdS), and CdSe QDs with total radii of 4.0 nm (**Figure 4f**). The agreement between theoretical and experimental trends remains if we change the simulations bandwidth to 75 meV, which is closer to the inhomogeneous broadening in the experiments (see SI).

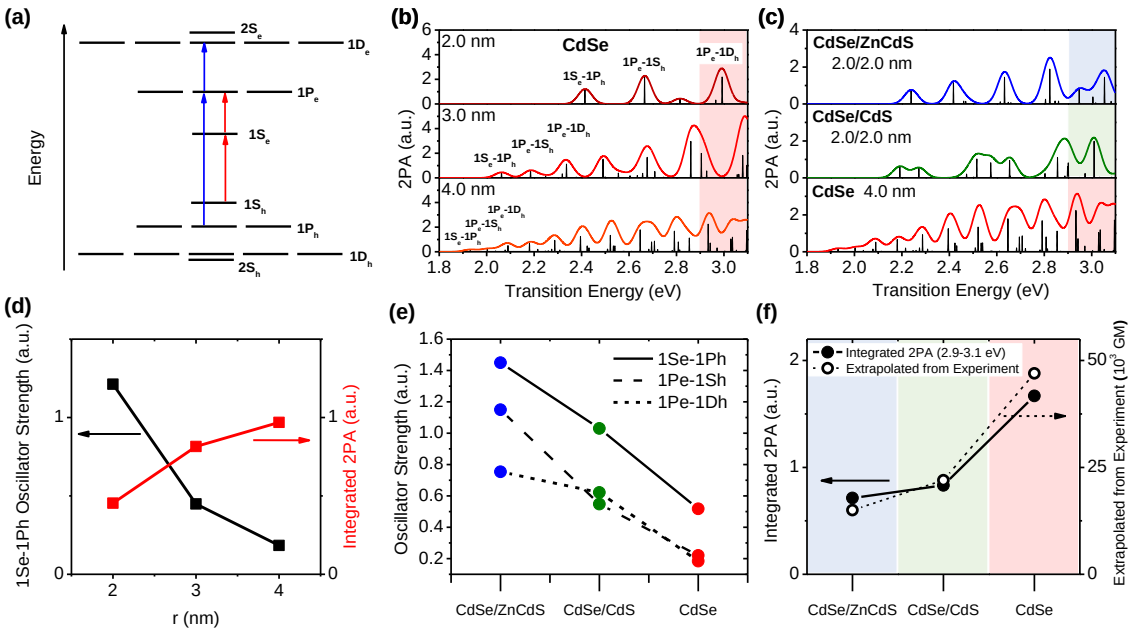

Figure 4. 2PA of core/shell NCs as inferred from electronic structure calculations. (a) Schematic of 2PA processes. The most relevant transitions involve initial (hole) and final (electron) states fulfilling $\Delta L=\pm 1$ (as in the blue and red arrows). (b) Calculated 2PA spectra for CdSe core-only

QDs with increasing radius. Sharp peaks correspond to discrete transitions, and the envelope band to a broadened spectrum to compare with the experiments. With increasing radius, the oscillator strength decreases but the DOS increases. (c) Calculated 2PA spectra for a CdSe QD (r = 4 nm), CdSe/ZnCdSe NC (r = 2.0 nm/H = 2.0 nm), and CdSe/CdS NC (r = 2.0 nm/H = 2.0 nm). The DOS in CdSe/CdS is intermediate between that of CdSe/ZnCdS and CdSe only. (d) Size dependence of the oscillator strength for transition $1S_e$ - $1P_h$ and of the W_{2PA} integrated over the quasi-continuum spectral range. (e) Dependence of the magnitude of the oscillator strength for the three first 2PA transition for different types of NCs with the same total radius (4.0 nm as in (c)). (f) Comparison of the predicted magnitude of W_{2PA} integrated over the quasi-continuum spectral range for the samples in (c) and the values obtained by extrapolating the experimental data from **Figure 3**.

According to the calculations, the density of final states should grow faster with the NCs volume when the shell is much thicker than the core. In fact, as shown in the supplementary material (**Figure S1**), for the CdSe/CdS data in **Figure 3**, if one considers only the first three data points, corresponding to samples with thinner shells, for that series, the slope is less steep than if one considers only the last three data points, corresponding to samples with thicker shells, suggesting that the volume dependence is weaker for thinner shells. This can be rationalized if one considers that for thinner shells, quasi-type-II heterostructures tend to present band alignment closer to that for type-I structures. Moreover, according to **Figure 3**, this band alignment represents a weaker volume dependence for σ_{2PA}. To verify that, we have investigated a second series of quasi-type-II CdSe/CdS heterostructures with a smaller core (core radius of 1.5 nm). Measurements of σ_{2PA} at 800 nm for three shell thicknesses indicate a steeper volume dependence, $\sigma_{2PA} \propto V^{0.89}$, similar to that for core only CdSe (**Figure 5a**). Comparing

these data to literature data taken at the same photon energy for CdS core-only nanomaterials,[21,22] we observe that they agree, indicating that, due to the large ratio between shell thickness and core radius, the 2PA process is dominated by the shell, which behaves effectively as a CdS core-only structure. Nevertheless, the emission is governed by the core, and consequently, this shows that it is possible to increase σ_{2PA} with a nearly linear dependence on the volume, while still maintaining the emission spectra almost unchanged, decoupling both properties and allowing for the manipulation of the NLO response without paying the price of shifting the emission spectra.

Figure 5b shows the decoupling between emission energy and the σ_{2PA} magnitude for quasi-type-II core/shell compared to core-only QDs. While for core-only an enhancement of one order of magnitude on σ_{2PA} corresponds to a PL peak shift larger than 400 meV, for the quasi-type-II heterostructure with 1.5 nm core a similar enhancement is obtained with a spectral shift of about 50 meV. This result indicates a path towards tailoring heterostructures to enhance σ_{2PA}, while keeping the emission at the same spectral range, which is relevant for applications of NCs as the active medium in 2PA-pumped lasers and as label for 3D imaging, for example.

While for application of NCs in 2PA-excited optical gain, enhancing σ_{2PA} is fundamental to reduce gain threshold, as this quantity depends on the number of excitons created per NC, for application of NCs as label for 3D-imaging, a more relevant parameter is the volume-normalized σ_{2PA}, as the resulting signal depends on the NC loading in the system to be imaged. The 2PA enhancement shown in **Figure 5b** is obtained at the expense of increasing the total NC volume and, from **Figure 5a**, it is evident that the volume-normalized σ_{2PA} is smaller for heterostructures than for core-only CdSe QDs. Nevertheless, in addition to enhanced σ_{2PA}, CdSe/CdS heterostructures, compared to

CdSe QDs, offer reduced inner filter effects,[32] and higher emission quantum efficiency, ϕ_{QY} (see Table S1 in the SI), which are advantageous for the applications mentioned above. Quantifying the influence of the inner filter effect is difficult because it depends on the optical density at the core $1S_e$-$1S_h$ peak (which depends on the NCs loading). Conversely, an appropriate Figure of Merit for this application, which accounts only for concentration-independent parameters, the volume-normalized σ_{2PA} and ϕ_{QY}, would be $F \equiv \frac{\sigma_{2PA}}{V_{NC}} \phi_{QY}$. **Figure 5c** shows F as a function of the emission energy for CdSe QDs and CdSe/CdS NCs, indicating the better performance of the heterostructures. One can also see that F is higher for heterostructures with thinner shells. This occurs because of the sublinear volume dependence of σ_{2PA}, and because ϕ_{QY} tends to decrease for thicker shells due to interfacial defects.[11]

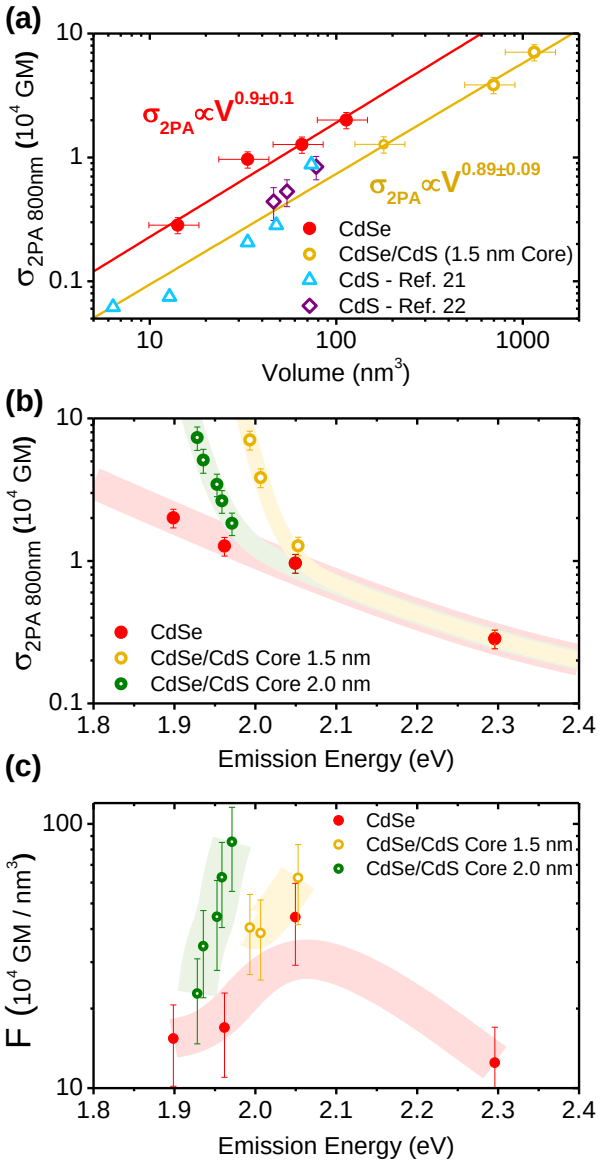

Figure 5. (a) Comparison of the volume dependence of σ_{2PA} between core only CdSe and CdS (CdS data from Ref. [21, 22]) and quasi-type-II CdSe/CdS with 1.5 nm core radius. (b) σ_{2PA} plotted as a function of the emission energy for core only and quasi-type-II core/shell evidencing that it is possible to decouple both properties by appropriated shell engineering. The shaded areas are simply guides to the eye. (c) Two-photon excited emission Figure of Merit, as defined in the text, plotted as a function of the emission energy for core only and core/shell NCs. The shaded areas are simply guides to the eye.

In conclusion, we have shown how different types of core/shell heterostructures influence the third-order NLO response of CdSe-based nanomaterials. The sublinear dependence of σ_{2PA} on the total nanoparticle volume originates from the reduced density of states in this type of nanomaterials. For CdSe/CdZnS, structures with type-I band alignment, the reduction in the density of final states is more dramatic as the initial and intermediate states are mostly on the core, being independent of the total volume. This reduction is less intense for quasi-type-II nanomaterials, tending to that of core-only structures when the shell volume is much larger than that of the core. Finally, our results indicate a path to decouple changes in the NLO response and shifts in the emission peak. This means that, by correctly choosing the ratio between core and shell dimensions, one can enhance the NLO response by about one order of magnitude, without drastically shifting the emission properties, opening new possibilities for applications that require materials with high nonlinear absorption, and emission, with high quantum yield at specific photon energies.

Supporting Information

Includes discussion on the experimental techniques used to obtain the 2PA cross section and spectra. Details of the experimental errors, and the MPAPS experimental data and fitting are displayed also, together with further discussion regarding the theoretical model, and the sample synthesis. This material is available free of charge via the Internet at http://pubs.acs.org.

Acknowledgments

This work has been funded by the São Paulo Research Foundation, FAPESP, under the grants 2018/15574-6, 2018/25339-4, and 2019/22823-5. AA and GN thank CNPq

(National Council for Scientific and Technological Development), and LWTB and JCL thank CAPES (Coordination of Superior Level Staff Improvement), for their Scholarship. JP, JLM, and JIC acknowledge support from UJI project UJI-B2021-06 and Generalitat Valenciana Prometeo project 22I235-CIPROM/2021/078.

References

(1) Schmitt-Rink, S.; Miller, D.; Chemla, D. S. Theory of the linear and nonlinear optical properties of semiconductor microcrystallites. *Phys. Rev. B* **1987**, *35*, 8113.

(2) Roussignol, P.; Ricard, D.; Flytzanis, C. Quantum confinement mediated enhancement of optical kerr effect in CdS x Se 1− x semiconductor microcrystallites. *Appl. Phys. B* **1990**, *51*, 437-442.

(3) Kataoka, T.; Tokizaki, T.; Nakamura, A. Mesoscopic enhancement of optical nonlinearity in CuCl quantum dots: Giant-oscillator-strength effect on confined excitons. *Phys. Rev. B* **1993**, *48*, 2815.

(4) Padilha, L. A.; Fu, J.; Hagan, D. J.; Van Stryland, E. W.; Cesar, C. L.; Barbosa, L. C.; Cruz, C. H. Two-photon absorption in CdTe quantum dots. *Opt. Express* **2005**, *13*, 6460-6467.

(5) Padilha, L.; Fu, J.; Hagan, D.; Van Stryland, E.; Cesar, C.; Barbosa, L.; Cruz, C.; Buso, D.; Martucci, A. Frequency degenerate and nondegenerate two-photon absorption spectra of semiconductor quantum dots. *Phys. Rev. B* **2007**, *75*, 075325.

(6) Qu, Y.; Ji, W. Two-photon absorption of quantum dots in the regime of very strong confinement: size and wavelength dependence. *J. Opt. Soc. Am. B* **2009**, *26*, 1897-1904.

(7) Padilha, L. A.; Nootz, G.; Olszak, P. D.; Webster, S.; Hagan, D. J.; Van Stryland, E. W.; Levina, L.; Sukhovatkin, V.; Brzozowski, L.; Sargent, E. H. Optimization of band structure and quantum-size-effect tuning for two-photon absorption enhancement in quantum dots. *Nano Lett.* **2011**, *11*, 1227-1231.

(8) Norris, D. J.; Efros, A. L.; Erwin, S. C. Doped nanocrystals. *Science* **2008**, *319*, 1776-1779.

(9) Brovelli, S.; Galland, C.; Viswanatha, R.; Klimov, V. I. Tuning radiative recombination in Cu-doped nanocrystals via electrochemical control of surface trapping. *Nano Lett.* **2012**, *12*, 4372-4379.

(10) Chen, Y.; Vela, J.; Htoon, H.; Casson, J. L.; Werder, D. J.; Bussian, D. A.; Klimov, V. I.; Hollingsworth, J. A. "Giant" multishell CdSe nanocrystal quantum dots with suppressed blinking. *J. Am. Chem. Soc.* **2008**, *130*, 5026-5027.

(11) Jeong, B. G.; Park, Y.-S.; Chang, J. H.; Cho, I.; Kim, J. K.; Kim, H.; Char, K.; Cho, J.; Klimov, V. I.; Park, P. Colloidal spherical quantum wells with near-unity photoluminescence quantum yield and suppressed blinking. *ACS Nano* **2016**, *10*, 9297-9305.

(12) Borys, N. J.; Walter, M. J.; Huang, J.; Talapin, D. V.; Lupton, J. M. The role of particle morphology in interfacial energy transfer in CdSe/CdS heterostructure nanocrystals. *Science* **2010**, *330*, 1371-1374.

(13) Rainò, G.; Stöferle, T.; Moreels, I.; Gomes, R.; Kamal, J. S.; Hens, Z.; Mahrt, R. F. Probing the wave function delocalization in CdSe/CdS dot-in-rod nanocrystals by time- and temperature-resolved spectroscopy. *ACS Nano* **2011**, *5*, 4031-4036.

(14) Bae, W. K.; Padilha, L. A.; Park, Y.-S.; McDaniel, H.; Robel, I.; Pietryga, J. M.; Klimov, V. I. Controlled alloying of the core–shell interface in CdSe/CdS quantum dots for suppression of Auger recombination. *ACS Nano* **2013**, *7*, 3411-3419.

(15) Nagamine, G.; Jeong, B. G.; Ferreira, T. A.; Chang, J. H.; Park, K.; Lee, D. C.; Bae, W. K.; Padilha, L. A. Efficient optical gain in spherical quantum wells enabled by engineering biexciton interactions. *ACS Photon.* **2020**, *7*, 2252-2264.

(16) Alo, A.; Barros, L. W.; Nagamine, G.; Vieira, L. B.; Chang, J. H.; Jeong, B. G.; Bae, W. K.; Padilha, L. A. Simple yet effective method to determine multiphoton absorption cross section of colloidal semiconductor nanocrystals. *ACS Photon.* **2020**, *7*, 1806-1812.

(17) Yang, Y. A.; Wu, H.; Williams, K. R.; Cao, Y. C. Synthesis of CdSe and CdTe nanocrystals without precursor injection. *Angew. Chem.* **2005**, *117*, 6870-6873.

(18) Lim, J.; Jeong, B. G.; Park, M.; Kim, J. K.; Pietryga, J. M.; Park, Y. S.; Klimov, V. I.; Lee, C.; Lee, D. C.; Bae, W. K. Influence of Shell Thickness on the Performance of Light-Emitting Devices Based on CdSe/$Zn_{1-X}Cd_XS$ Core/Shell Heterostructured Quantum Dots. *Adv. Mater.* **2014**, *26*, 8034-8040.

(19) Makarov, N. S.; Lau, P. C.; Olson, C.; Velizhanin, K. A.; Solntsev, K. M.; Kieu, K.; Kilina, S.; Tretiak, S.; Norwood, R. A.; Peyghambarian, N. Two-photon absorption in CdSe colloidal quantum dots compared to organic molecules. *ACS Nano* **2014**, *8*, 12572-12586.

(20) Pu, S. C.; Yang, M. J.; Hsu, C. C.; Lai, C. W.; Hsieh, C. C.; Lin, S. H.; Cheng, Y. M.; Chou, P. T. The empirical correlation between size and two-photon absorption cross section of CdSe and CdTe quantum dots. *Small* **2006**, *2*, 1308-1313.

(21) Achtstein, A. W.; Hennig, J.; Prudnikau, A.; Artemyev, M. V.; Woggon, U. Linear and two-photon absorption in zero-and one-dimensional CdS nanocrystals: influence of size and shape. *J. Phys. Chem. C* **2013**, *117*, 25756-25760.

(22) Li, X.; van Embden, J.; Chon, J. W.; Gu, M. Enhanced two-photon absorption of CdS nanocrystal rods. *Appl. Phys. Lett.* **2009**, *94*, 103117.

(23) Nagamine, G.; Rocha, J. O.; Bonato, L. G.; Nogueira, A. F.; Zaharieva, Z.; Watt, A. A.; de Brito Cruz, C. H.; Padilha, L. A. Two-photon absorption and two-photon-induced gain in perovskite quantum dots. *J. Phys. Chem. Lett.* **2018**, *9*, 3478-3484.

(24) Sousa, C. A.; Bonato, L. G.; Gonçalves, E. S.; Alo, A.; Vale, B. R. C.; Almeida, D. B.; Nogueira, A. F.; Zagonel, L. F.; Padilha, L. A. Addressing the Magnitude of the Nonlinear Refraction Response in Perovskite Nanocrystals. *ACS Photon.* **2023**, *10*, 1334-1340.

(25) Xu, C.; Webb, W. W. Measurement of two-photon excitation cross sections of molecular fluorophores with data from 690 to 1050 nm. *J. Opt. Soc. Am. B* **1996**, *13*, 481-491.

(26) Achtstein, A. W.; Ballester, A.; Movilla, J. L.; Hennig, J.; Climente, J. I.; Prudnikau, A.; Antanovich, A.; Scott, R.; Artemyev, M. V.; Planelles, J. One-and two-photon absorption in CdS nanodots and wires: the role of dimensionality in the one-and two-photon luminescence excitation spectrum. *J. Phys. Chem. C* **2015**, *119*, 1260-1267.

(27) Schmidt, M. E.; Blanton, S. A.; Hines, M. A.; Guyot-Sionnest, P. Size-dependent two-photon excitation spectroscopy of CdSe nanocrystals. *Phys. Rev. B* **1996**, *53*, 12629.

(28) Allione, M.; Ballester, A.; Li, H.; Comin, A.; Movilla, J. L.; Climente, J. I.; Manna, L.; Moreels, I. Two-photon-induced blue shift of core and shell optical transitions in colloidal CdSe/CdS quasi-type II quantum rods. *ACS Nano* **2013**, *7*, 2443-2452.

(29) Heckmann, J.; Scott, R.; Prudnikau, A. V.; Antanovich, A.; Owschimikow, N.; Artemyev, M.; Climente, J. I.; Woggon, U.; Grosse, N. B.; Achtstein, A. W. Directed two-photon absorption in CdSe nanoplatelets revealed by k-space spectroscopy. *Nano Lett.* **2017**, *17*, 6321-6329.

(30) Planelles, J.; Achtstein, A. W.; Scott, R.; Owschimikow, N.; Woggon, U.; Climente, J. I. Tuning intraband and interband transition rates via excitonic correlation in low-dimensional semiconductors. *ACS Photon.* **2018**, *5*, 3680-3688.

(31) Blanton, S. A.; Hines, M. A.; Schmidt, M. E.; Guyot-Sionnest, P. Two-photon spectroscopy and microscopy of II–VI semiconductor nanocrystals. *J. Lumin.* **1996**, *70*, 253-268.

(32) Meinardi, F.; Colombo, A.; Velizhanin, K. A.; Simonutti, R.; Lorenzon, M.; Beverina, L.; Viswanatha, R.; Klimov, V. I.; Brovelli, S. Large-area luminescent solar concentrators based on 'Stokes-shift-engineered' nanocrystals in a mass-polymerized PMMA matrix. *Nat. Photon.* **2014**, *8*, 392-399.

ToC Graphic